Supporting Information

Non-Radical Dominated PMS Activation by High-Entropy Alloy for Water Decontamination

Youzhong Hu[1,#], Jinli Chen[1,#], Hanwen Liu[1], Wenhui Shi[1,*], Wei Wang[1,2], Fatang Tan[1,2], Xiaodong Chi[1], Yonggang Yao[1,2,*]

[1]State Key Laboratory of Materials Processing and Die & Mould Technology, School of Materials Science and Engineering, Huazhong University of Science and Technology, Wuhan, 430074 China
[2]Shenzhen Huazhong University of Science and Technology Research Institute, Shenzhen, 518000, China

Email: yaoyg@hust.edu.cn, shiwenhui@hust.edu.cn

Experimental

Chemicals. Cobalt chloride hexahydrate ($CoCl_2 \cdot 6H_2O$, 99.9%), iron chloride tetrahydrate ($FeCl_2 \cdot 4H_2O$, 98%), nickel chloride hexahydrate ($NiCl_2 \cdot 6H_2O$, 99%), copper chloride tetrahydrate ($CuCl_2 \cdot 4H_2O$, 98%), manganese chloride tetrahydrate ($MnCl_2 \cdot 4H_2O$, 99%), Rhodamine B (RhB, 99%), sulfamethoxazole (SMX, 98%), 4-Chlorophenol (4-CP, 98%), Phenol (Phenol, 99.0%), peroxymonosulfate ($2KHSO_5 \cdot KHSO_4 \cdot K_2SO_4$, 98%), methanol (MeOH, 99.9%), furfuryl alcohol (FFA, 98%), tertiary butyl alcohol (TBA, 99.5%), ethanol (EtOH, 99.8%), iso-propanol (99.8%), sodium sulfate anhydrous (Na_2SO_4, 99%), sodium nitrate ($NaNO_3$, 99%), sodium bicarbonate ($NaHCO_3$, 99.5%), sodium chloride (NaCl, 99.5%), humic acid (HA, 90%), sodium thiosulfate ($Na_2S_2O_3$, 99%), 5,5-dimethyl-1-pyrroline-N-oxide (DMPO, 97%), and 2,2,6,6-tetramethylpiperidine (TEMP, 97%), were purchased from Macklin (Shanghai, China). Carbon paper (HCP030N) and carbon black (CB, XC-72R) were purchased from Taobao. All solvents and reagents were obtained from commercial sources and were used without further purification.

Synthesis of HEA. Prepare separate 0.2 M ethanolic solutions of $CoCl_2$, $FeCl_2$, $CuCl_2$, $NiCl_2$, and $MnCl_2$ for later use. Following the proportions outlined in Table S1, mix the precursor solutions (500 μL for each sample), and then drop them onto 25 mg of CB and grind evenly. Dry the CB with the precursor at 105 °C. After drying, spread the carbon black with the precursor evenly on the CTS device (Firstly, Carbon felt was cut into 5 × 3 cm^2 pieces, folded to 5 × 1.5 cm^2, and clamped between two electrodes to form a carbon felt heating chamber. Then, the CB powders loaded with salt precursors were added to the chamber. Finally, Joule heating was applied by passing a series of currents in an argon atmosphere, and the synthesis temperature was monitored using an infrared probe). All samples are heated at approximately 1400 °C for 1 s.

Characterization. The morphologies of HEA have been obtained through transmission electron microscopy (TEM, Prochips 200). The structural information was characterized by X-ray diffraction (XRD, Rigaku miniflex-600), and Raman spectrum (Raman, LabRAM HR800). The surface area of HEA was characterized by Brunauer–Emmett–Teller (BET, ASAP2420-4MP)

Catalytic performance evaluation. Pollutant degradation experiment, a 25 mL beaker containing pollutant (RhB, SMX, 4-CP, phenol, 20 mg L^{-1}) and HEA catalyst (0.1 g L^{-1}), after 30 min stirred for maximum adsorption, the PMS (0.15 g L^{-1}) was added to the reaction system. At 3 min intervals, 1 ml of the solution was siphoned from the reaction system, then the solution was added into a centrifuge tube with 1ml 0.1 M $Na_2S_2O_3$ to quench the reaction. After being filtered through a microporous membrane (0.45 μm), the RhB was analyzed by the Ultraviolet-visible spectrometer (UV-Vis, UV 2600), SMX, 4-CP, and phenol were analyzed using high-performance liquid chromatography (HPLC, Agilent 1100, USA).

To evaluate the contribution of radicals and $^1O_2$ to pollutant degradation, 160 μL MeOH (0.5 M), 480 μL TBA (0.5 M), and 50 μL FFA (0.03 M) served as the trapping agent of $\cdot OH + \cdot SO_4^-$, $\cdot SO_4^-$, and $\cdot OH + \cdot SO_4^- + {}^1O_2$, respectively. Further, the electron paramagnetic resonance (EPR) spectrum was adopted to prove the existence of $\cdot OH + \cdot SO_4^- + {}^1O_2$. The DMPO and TEMP were used as capture agents to determine $\cdot OH + \cdot SO_4^-$ and $^1O_2$, respectively.

Preparation of the catalyst ink: Mix 5 mg HEA/CB with 800 μL of DI water and 200 μL of isopropanol, then disperse with an ultrasonic disruptor for 20 min. Afterward, add 20 μL of 5% Nafion and disperse again with an ultrasonic disruptor for another 20 min. Apply 10 μL of the catalyst ink onto the glassy carbon electrode, allow it to air dry naturally, and then use it as the working electrode. The electrochemical workstation (CORRTEST CS6) was used to perform electrochemical detections to measure the electron transfer direction between PMS/catalyst/pollutant using a three-electrode system consisting of a graphite counter electrode and a saturated Ag/AgCl reference electrode, 0.5 M Na_2SO_4 solution as electrolyte. The

PMS solution or the mixed solution of PMS and RhB was injected after scanning for 30 s at the open potential, the mixing concentration of PMS was 0.2 g L^{-1} and the concentration of RhB solution was 20 ppm.

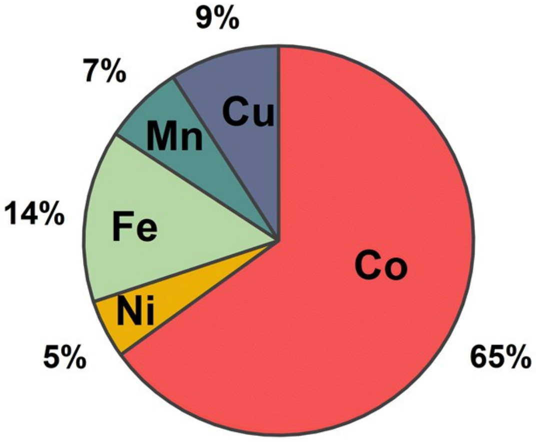

Fig. S1. The metal element ratio in the HEA catalyst.

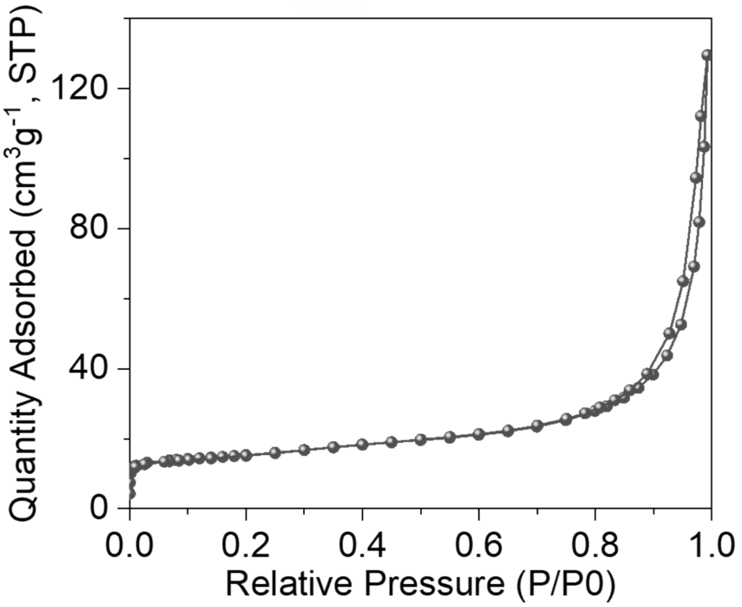

Fig. S2. BET curve of $Co_{55}Fe_{15}$ HEA.

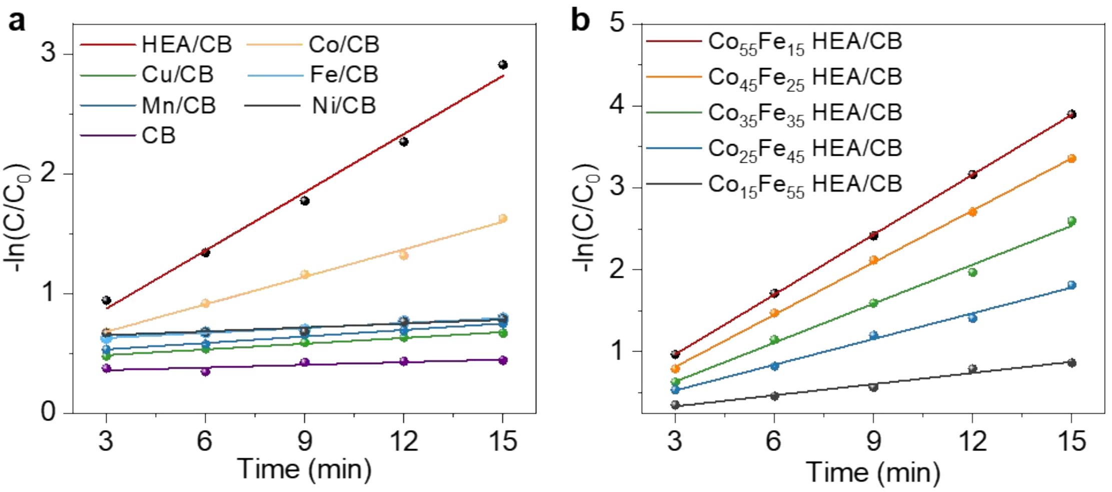

Fig. S3. (a) The kinetic fitting curve of $Co_{35}Fe_{35}$ HEA, unitary metal complex and joule heating treated CB sample. **(b)** Different fractions of HEA.

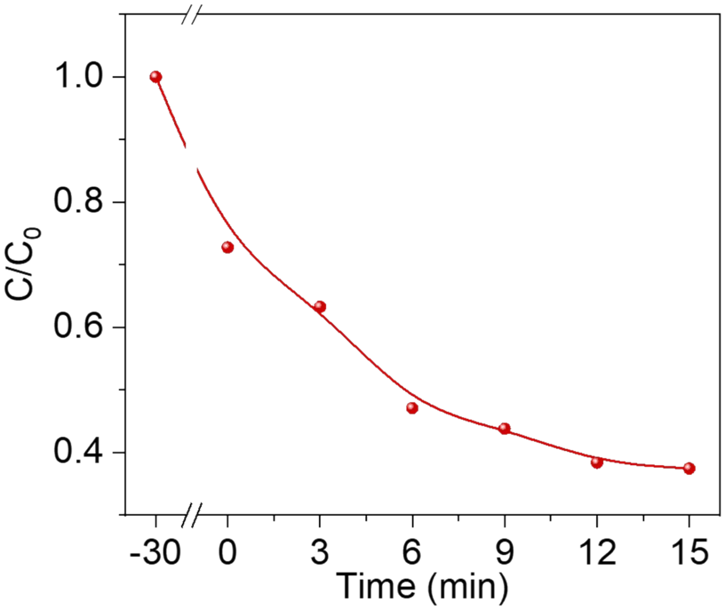

Fig. S4. TOC curve during the RhB degradation process.

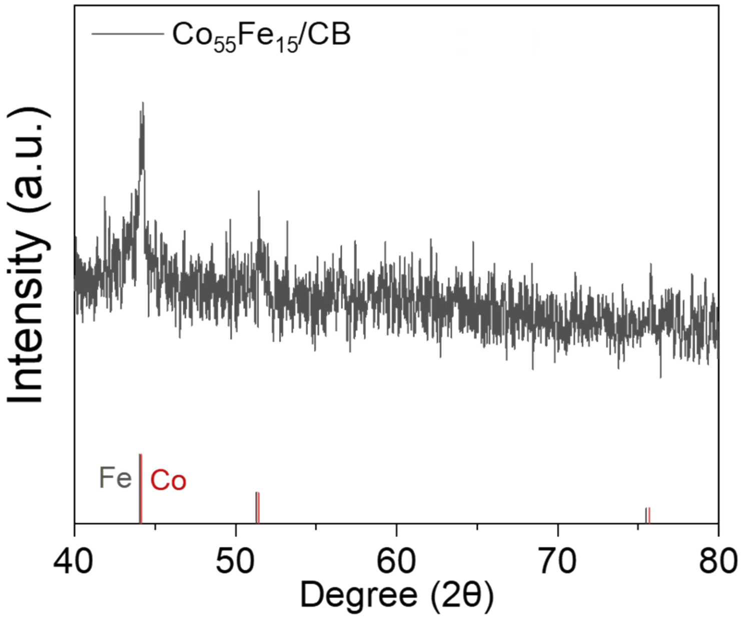

Fig. S5. XRD curve of $Co_{55}Fe_{15}$.

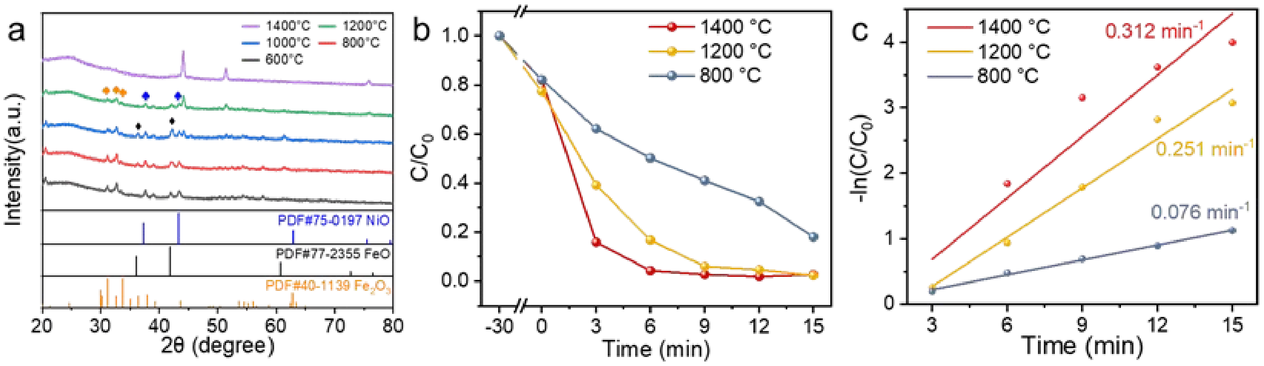

Fig. S6. (a) Influence of different synthesis temperatures on the phase composition of the catalyst. **(b), (c)** Degradation performance and kinetic parameters of catalysts synthesized at different temperatures. [RhB] = 20 ppm, [catalyst] = 0.1 g L^{-1}, [PMS] = 0.15 g L^{-1}.

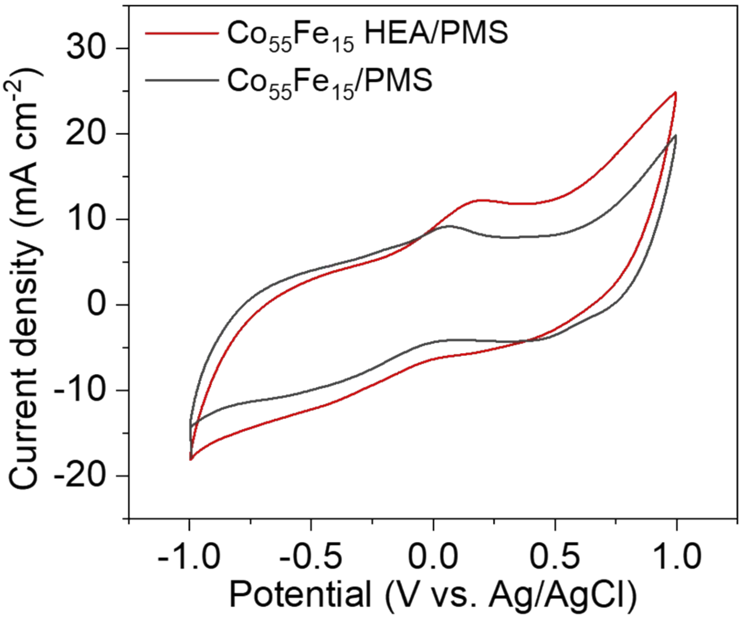

Fig. S7. CV curves of $Co_{55}Fe_{15}$ HEA and $Co_{55}Fe_{15}$ in the presence of PMS.

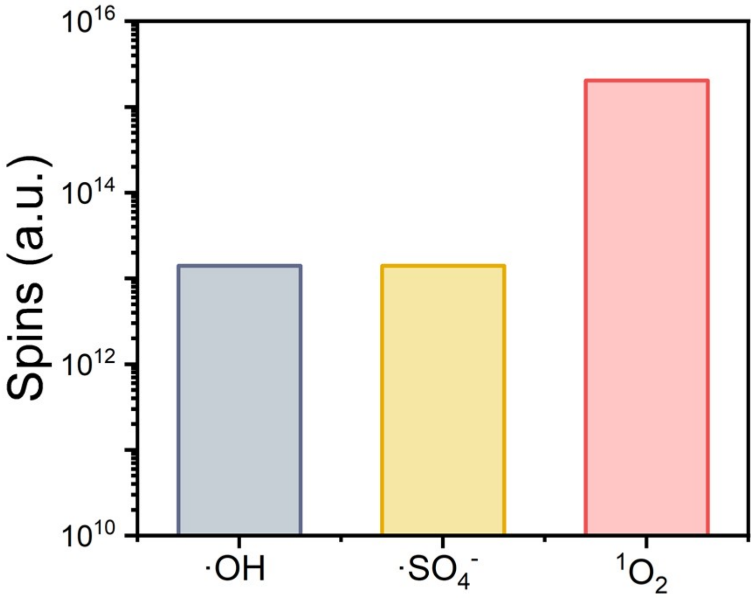

Fig. S8. Spin concentrations of the different reactive species.

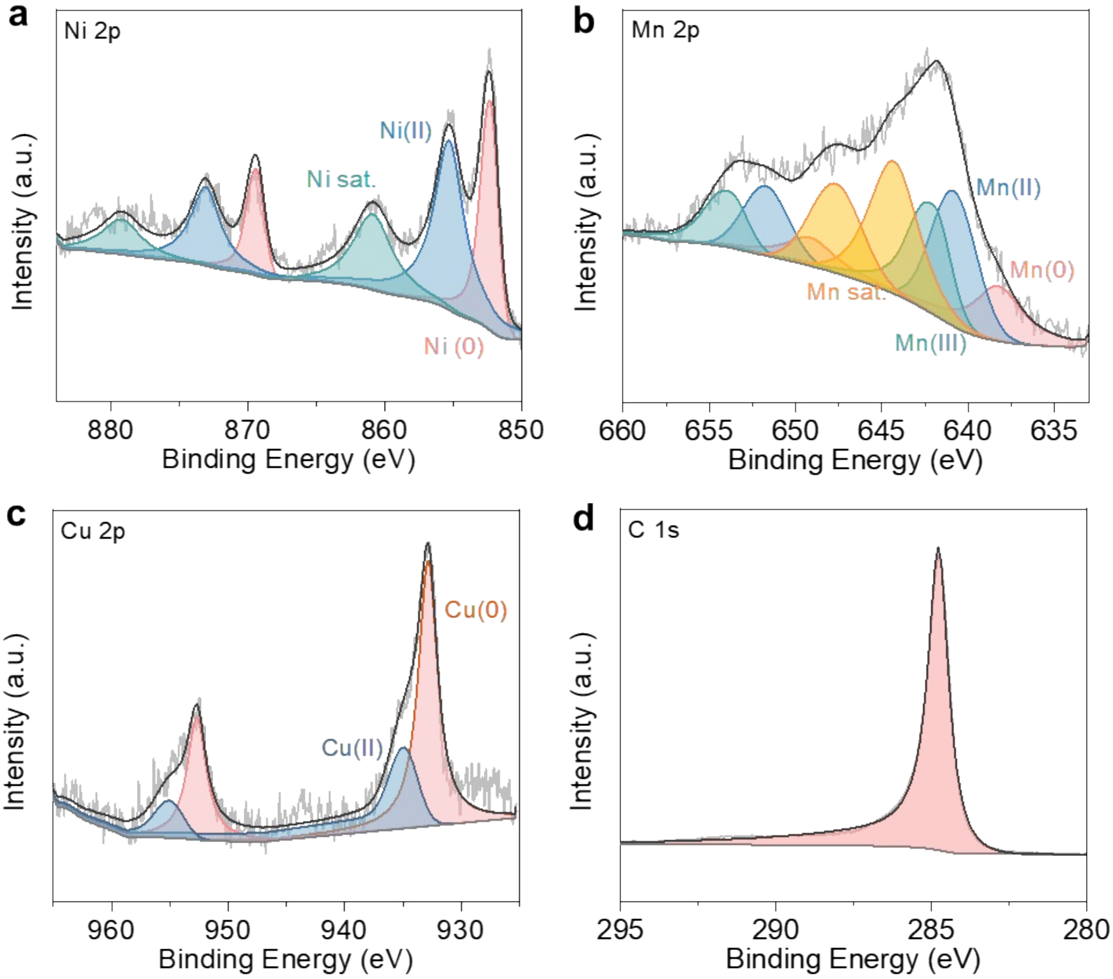

Fig. S9. XPS characterization of activated $Co_{55}Fe_{15}$ HEA surface.

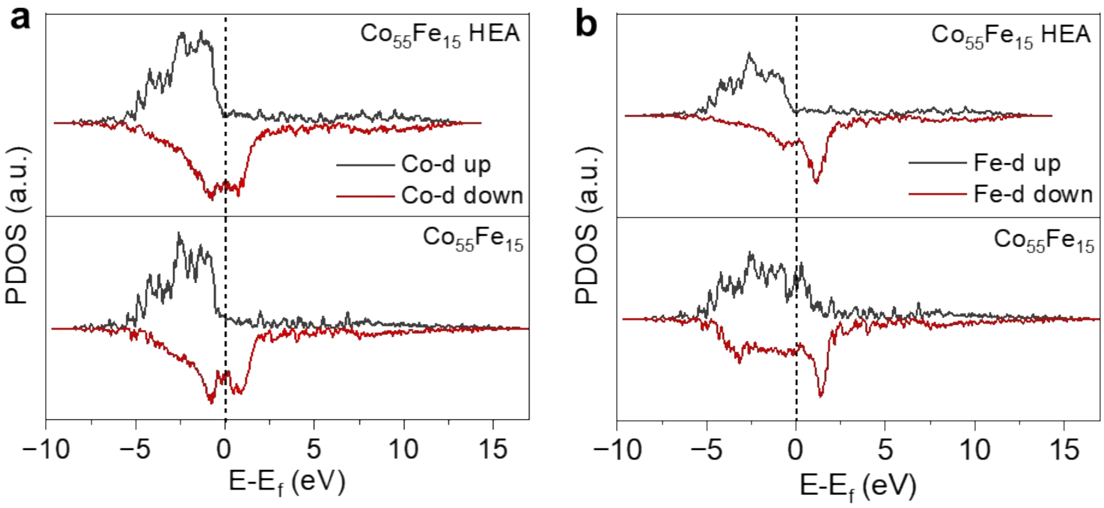

Fig. S10. The density of states of **(a)** Co and **(b)** Fe on $Co_{55}Fe_{15}$ HEA and $Co_{55}Fe_{15}$ surfaces.

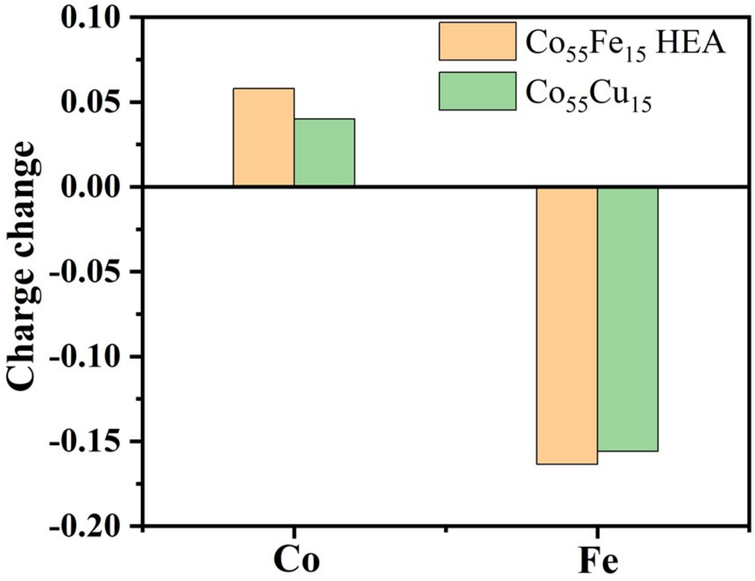

Fig. S11. Charge variations of Co and Fe in the HEA and binary alloys.

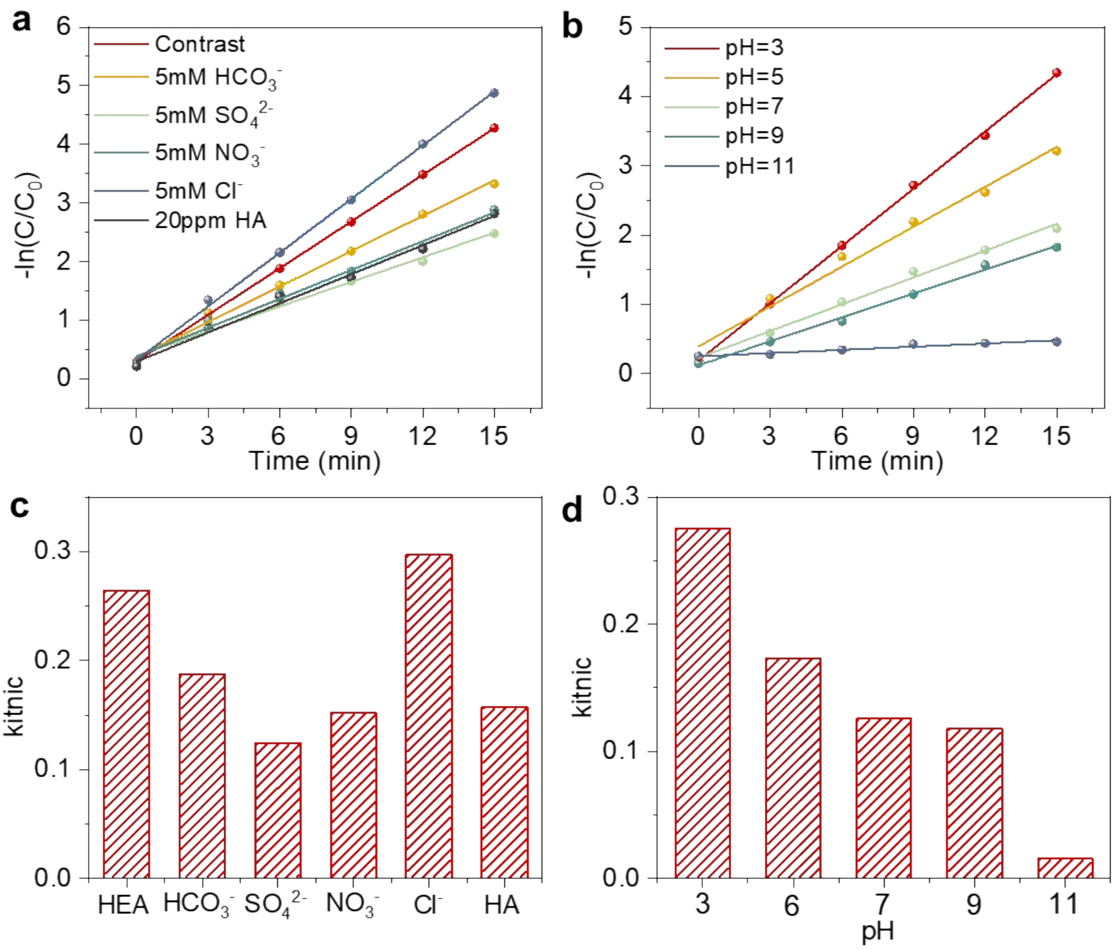

Fig. S12. The kinetic fitting curves of (**a**) different impurities added. (**b**) at different pH. The comparison of kinetic constants of (**c**) different impurities added. (**b**) at different pH.

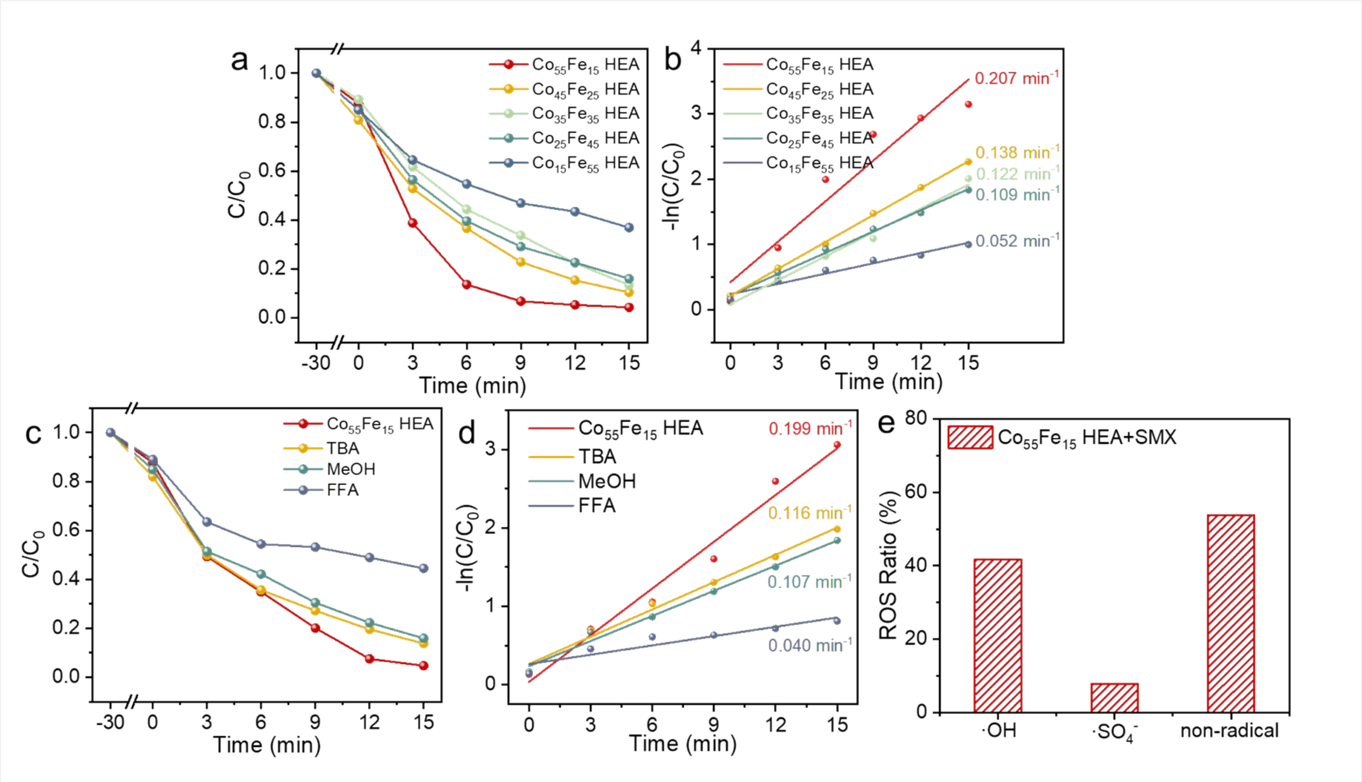

Fig. S13. (a), **(b)** Performance and kinetic parameters of different HEA catalysts for SMX degradation. **(c)**, **(d)** Effects of different quenchers on the degradation performance and kinetic parameters of $Co_{55}Fe_{15}$ HEA catalyst. **(e)** Comparison of different ROS contents in SMX degradation process. [SMX] = 20 ppm, [catalyst] = 0.1 g L^{-1}, [PMS] = 0.15 g L^{-1}.

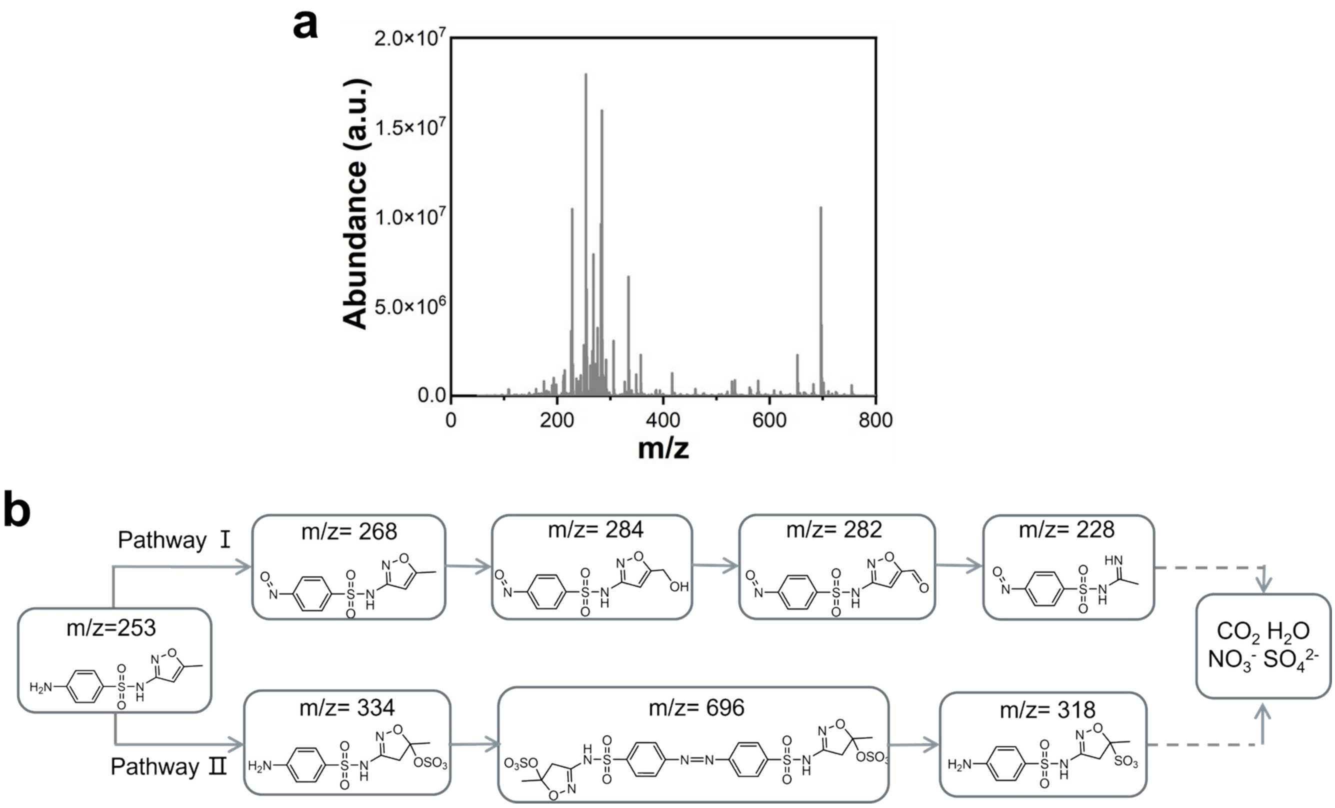

Fig. S14. Reaction intermediates detected by HPLC-MS and inference of smx degradation pathway. **(a)** The mass spectrometry of the possible intermediate products. **(b)** SMX degradation pathway inferred from HPLC-MS results.

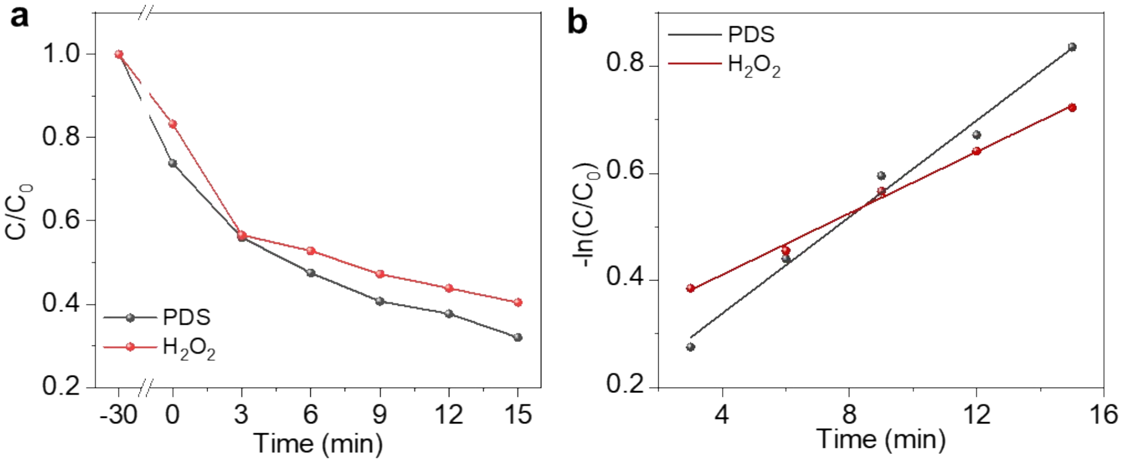

Fig. S15. The curve of $Co_{55}Fe_{15}$ HEA activating PDS or H_2O_2 for the degradation of RhB.

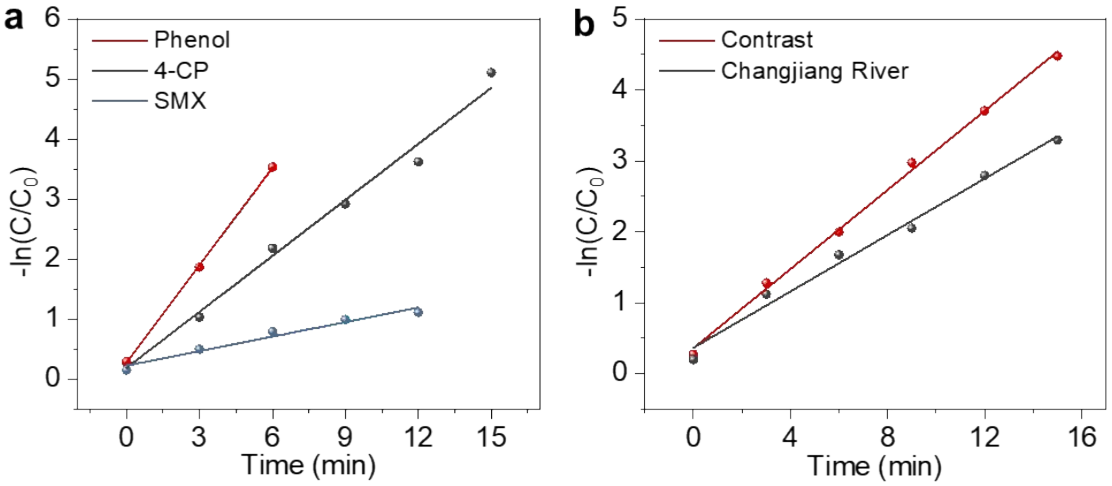

Fig. S16. The kinetic fitting curves of **(a)** different pollutants and **(b)** RhB by using Changjiang River water.

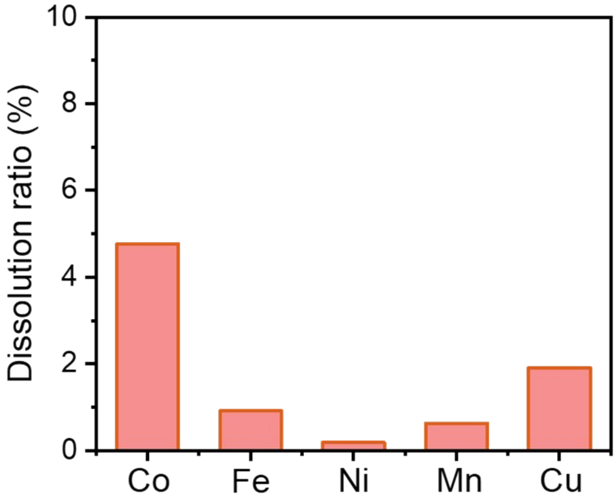

Fig. S17. The metal leaching rates of the $Co_{55}Fe_{15}$ HEA catalyst after participating in the degradation reaction for 15 min.

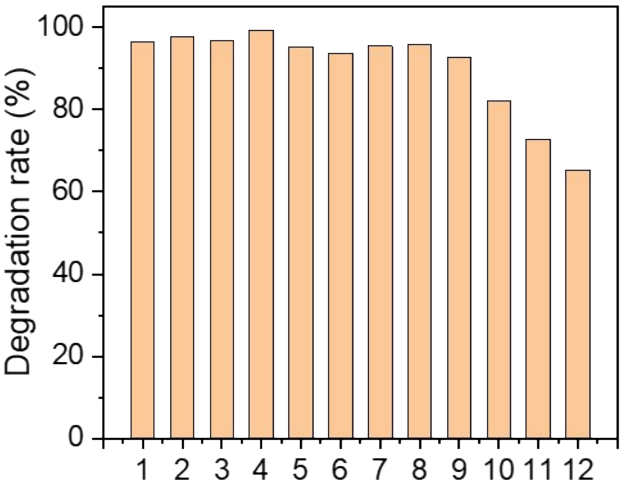

Fig. S18. RhB degradation curves after recycling the HEA 12 times.

Table S1. The denotation of the Representative Catalysts.

	Atom ratio **(Co:Fe:Ni:Mn:Cu)**	**Volume ratio** **(Co:Fe:Ni:Mn:Cu) µL/25mg CB**
$\mathbf{Co_{55}Fe_{15}Ni_{10}Mn_{10}Cu_{10}}$	55:15:10:10:10	275:75:50:50:50
$\mathbf{Co_{45}Fe_{25}Ni_{10}Mn_{10}Cu_{10}}$	45:25:10:10:10	225:125:50:50:50
$\mathbf{Co_{35}Fe_{35}Ni_{10}Mn_{10}Cu_{10}}$	35:35:10:10:10	175:175:50:50:50
$\mathbf{Co_{25}Fe_{45}Ni_{10}Mn_{10}Cu_{10}}$	25:45:10:10:10	125:225:50:50:50
$\mathbf{Co_{15}Fe_{55}Ni_{10}Mn_{10}Cu_{10}}$	15:55:10:10:10	75:275:50:50:50
$\mathbf{Co_{55}Fe_{15}}$	55:15:0:0:0	390:110:0:0:0